Microwave On-Chip Bandpass Filter Based on Hybrid Coupling Technique

Mengze Li, *Student Member, IEEE,* Yang Yang, *Senior Member, IEEE,* Kai Da Xu, *Member, IEEE,* Xi Zhu, *Member, IEEE,* and Sai Wai Wong, *Senior Member, IEEE*

***Abstract*—In this paper, a novel on-chip circuit design approach is proposed using hybrid coupling technique. Taking advantage of this technique, a microwave bandpass filter (BPF) is proposed as a design example for proof-of-concept. Based on stub-loaded stepped-impedance transmission lines (TLs) and folded stepped-impedance meander line from different metal layers, the proposed BPF can generate three transmission zeros (TZs) and two transmission poles (TPs), which are excited through the hybrid mutual couplings between the inductive and capacitive metals. To understand the principle of this configuration, an equivalent *LC*-circuit model is presented and simplified, of which the TZs and TPs of the proposed BPF are estimated by the extracted transfer function. The calculated results exhibit good agreements with the simulated and measured ones. In addition, the bandwidth and center frequency of the proposed BPF can be tuned flexibly. Finally, to further demonstrate the feasibility of this approach in practice, the structure is implemented and fabricated in a commercial 0.13-μm SiGe (Bi)-CMOS technology. The measurement results show that the proposed BPF, whose chip size is 0.39 mm × 0.45 mm (excluding the test pads), can realize a wide bandwidth from 19.7 GHz to 33.2 GHz with return loss of 15.8 dB and insertion loss of 3.8 dB at the center frequency of 26.5 GHz.**

***Index Terms*—Bandpass filter (BPF), capacitive coupling, magnetic coupling, microwave, mutual coupling, on-chip devices.**

I. Introduction

In the past decades, design of high-performance integrated circuits operated at the so-called microwave region has attracted enormous attentions. Taking advantage of the fact that low-loss and compact passive structures can be fully integrated with active devices on the same chip, many advanced building blocks, such as power dividers [1], antennas [2], rectennas [3], and bandpass filters (BPFs) [4]-[9], have been successfully implemented in advanced semiconductor technologies. In wideband application systems, such as ultra-wideband communication systems and sensing systems, local oscillator is required to be designed with a wide frequency tuning range, which may require the designed BPF with relatively wide bandwidth [10-11]. It is desired to effectively utilize the provided multi-metal layers to achieve advanced features such as multi-mode [12] or multi-order [13] constructions. Nevertheless, these steps compose a challenge in microwave IC designs, because the mutual coupling techniques play a significant role on performance elevation of not only a single circuit element but also the whole system.

Admittedly, mutual coupling is an inevitable interaction among different building blocks as well as devices, particularly, with passive devices laid in a dense area. As an important technique, mutual coupling can be used for various implementation of circuits where advances are desired with the features of multiple transmission zeros (TZs), multiple transmission poles (TPs) for the measure of wide bandwidth, sharp roll-off and superior harmonic suppression with compact layout and low insertion loss. However, mutual coupling is complex for the microwave on-chip circuit designs. It might bring undesirable parasitic effects among metals and crossing layers, consequently degrading the overall performance of the system.

As an indispensable step, an accurate and effective equivalent circuit model is the foundation of applying mutual coupling techniques [14]-[20]. In [17]-[18] two ultra-compact BPFs based on a pair of broadside-coupling meander lines are designed and analyzed with their equivalent circuits, where the inductive coupling is represented by coupling coefficient and the capacitive coupling by lumped capacitors. However, there are still limitations in terms of the number of TPs and TZs [17] and out-of-band rejection [18]. In [19]-[20], the magnetic mutual couplings are represented by metal inductors indicating a promising solution for microwave on-chip circuit designs. Nevertheless, the presented coupling technique is based on edge-coupled structures in III-V technologies, which might not be an effective solution in Silicon technologies. The loss tangent of a typical Silicon substrate is 10 times higher than its III-V counterparts. Moreover, a commercial III-V process only has one metal layer for design, of which the strictly required full ground configuration is fully-different from the commercial CMOS technologies. Therefore, the mutual coupling techniques are expected to be well studied for achieving the advanced features with minimized side effects from parasitic and lossy substrate.

To effectively apply the mutual coupling techniques into a complex on-chip circuit design, this paper introduces a generic circuit analysis and design approach, which can predict mutual coupling behaviors between passive structures. Using the proposed hybrid coupling techniques, the designed BPF can realize three TZs and two TPs at the

This work was supported in part by the National Natural Science Foundation of China under Grant 61601390, and in part by the Shenzhen Science and Technology Innovation Project under Grant JCYJ20170306141249935 (corresponding author Kai Da Xu, e-mail: kaidaxu@xmu.edu.cn)

M. Li, and K. D. Xu are with the Department of Electronic Science, Xiamen University, Xiamen 361005, and also with the Shenzhen Research Institute of Xiamen University, Shenzhen 518057, China.

Y. Yang and X. Zhu are with the School of Electrical and Data Engineering, University of Technology Sydney, Ultimo, NSW 2007, Australia.

S. W. Wong is with the College of Information Engineering, Shenzhen University, Shenzhen 518060, China.

designed frequencies. An equivalent circuit of the designed BPF is demonstrated interpreting the magnetic and capacitive coupling effects. For verification, a novel BPF employing hybrid coupling techniques is implemented and fabricated in a standard 0.13-µm SiGe (Bi)-CMOS technology. The designed BPF has the capability of independent frequency-tuning of the realized TZs and TPs, as a result of the mutual coupling effect, which approves that the bandwidth and center frequency of proposed BPF can be adjusted flexibly. The two TPs and three TZs are formulated, of which the calculated resonant frequencies indicate good agreement with the simulated results of both the electromagnetic (EM) structure and equivalent circuit model. The measured results of the proposed BPF show competitive performance compared with the state-of-the-art works [5], [9], [12]-[13], [18] and [20].

II. BPF Using Hybrid Coupling Technique

A. *Bandpass Filter Overview*

In Fig. 1(a), the metal stack-up of the selected 0.13-µm SiGe (Bi)-CMOS technology is presented. Seven metal layers and metal-insulator-metal (MIM) capacitor are available for circuit design. The MIM layer is located between TM1 and M5. In this work, the TM2, TM1 and M1 layers are employed to design the BPF, where M1 is used as the RF ground. The TM2 and TM1 layers are utilized to realize the hybrid coupling. The 3-D view of TM2 and TM1 layers of the designed BPF is depicted in Fig. 1(b). The top two metal layers with conductance of 3.03×10^7 S/m (metal thickness of 3 µm) and 2.78×10^7 S/m (metal thickness of 2 µm), respectively, are used to construct the signal path of the BPF. Two loaded metal stubs on the TM2 are connected to the shielding ground, which are not given in Fig. 1(b) for a better visibility. To construct the shielding ground, all metal layers are stacked. The layouts of TM2 and TM1 layers are shown in Fig. 1(c) and (d), respectively. Fig. 1(e) shows the 2-D view of the BPF with shielding ground. As illustrated, the presented BPF consists of two stepped-impedance transmission lines (TLs) loaded with an open-ended bending stub and a short-ended one on the top metal layer TM2, as well as a folded stepped-impedance meander line on the second metal layer TM1. The physical dimensions of the proposed BPF are tabulated in Table I.

TABLE I
DIMENSIONS OF THE PROPOSED BPF

Symbol	W	W_1	W_2	W_3	W_4
Value	15µm	9µm	8µm	9µm	40µm
Symbol	W_5	W_6	L	L_1	L_2
Value	36µm	10µm	60µm	140µm	66µm
Symbol	L_3	L_4	L_5	L_6	L_7
Value	132µm	34µm	32µm	220µm	170µm
Symbol	L_8	L_9	L_{10}	L_{11}	L_{12}
Value	38µm	160µm	210µm	16µm	115µm
Symbol	L_{13}	L_{14}	L_{15}	S	S_1
Value	110µm	36µm	282µm	6µm	6µm

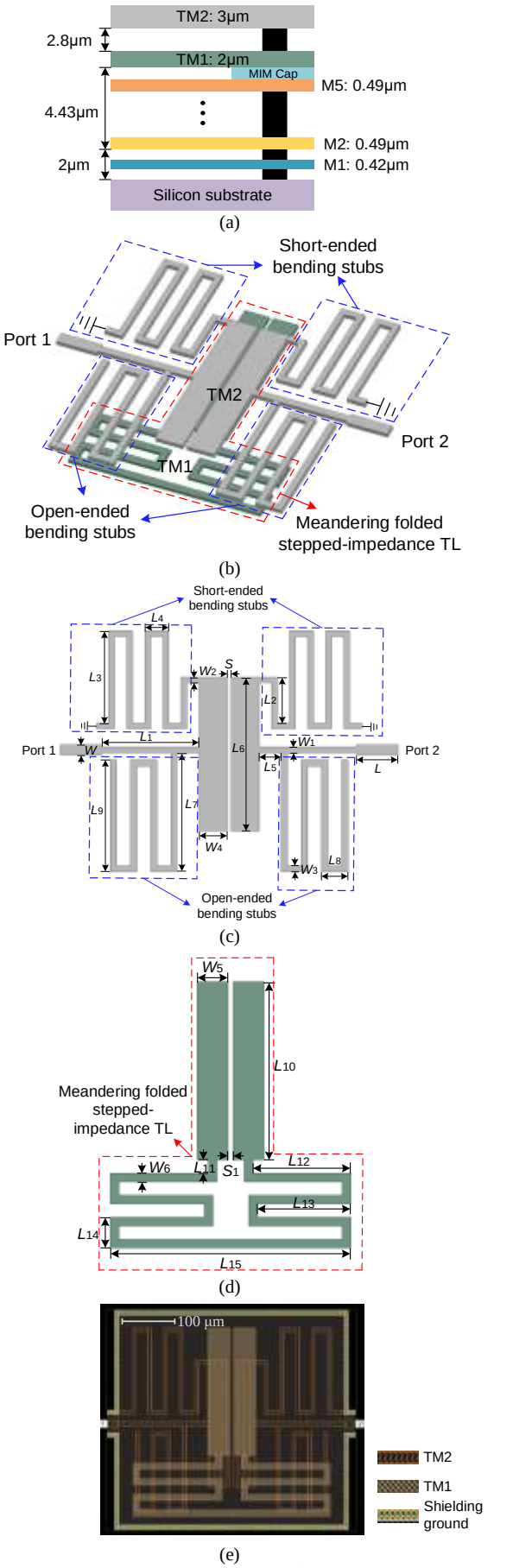

Fig. 1. Designed BPF: (a) metal stack-up of the applied 0.13-µm SiGe (Bi)-CMOS technology, (b) 3-D view of TM2 and TM1 layers, (c) 2-D view of TM2 layer, (d) 2-D view of TM1 layer, and (e) 2-D view of the presented structure with shielding.

B. *Hybrid Coupling Technique in Extraction of Equivalent LC-Circuit Model*

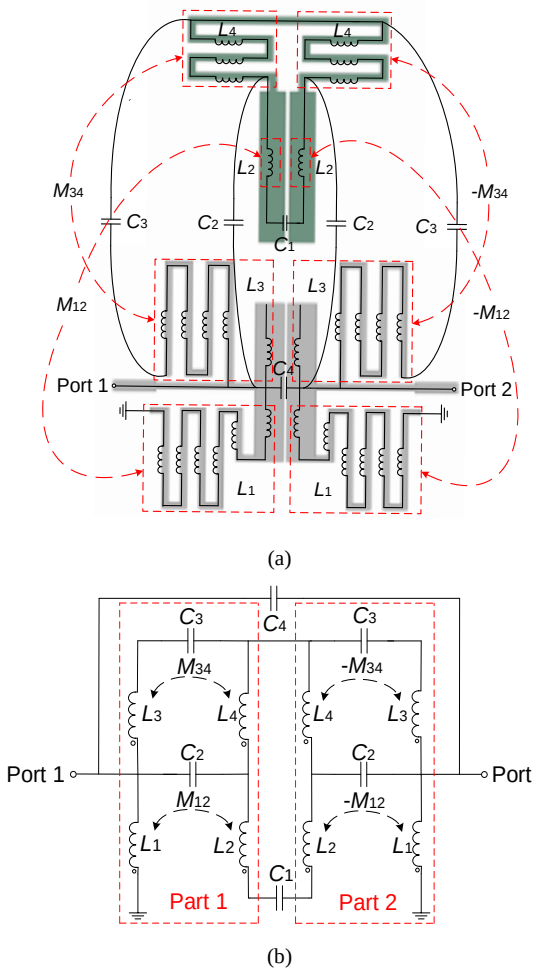

Fig. 2. (a) Equivalent *LC*-circuit model based on layout and (b) simplified one of the proposed BPF.

To facilitate the analysis of the proposed on-chip BPF, an equivalent circuit based on hybrid coupling technique is presented and discussed. Fig. 2(a) presents the equivalent *LC*-circuit model of the presented EM structure, where the high-impedance lines and the capacitive couplings are represented by inductors and capacitors, respectively. Inductors connected in series or parallel can be merged into one inductor element represented as the self-inductance L_i (i=1, 2, 3, 4). Moreover, the hybrid couplings between the two metal layers are shown as capacitors and mutual inductors representing the capacitive and magnetic couplings, respectively. As shown in Fig. 2(a), the mutual inductance between L_1 and L_2 is denoted by M_{12}, while the mutual inductance between L_3 and L_4 is represented by M_{34}. C_1 and C_4 represent the capacitive couplings between different TLs in the same layer. C_2 and C_3 represent the capacitive couplings between TM2 and TM1 layers. Furthermore, the equivalent *LC*-circuit model of the proposed BPF is simplified as demonstrated in Fig. 2(b).

C. *Analysis of Equivalent LC-Circuit Model*

For circuit analysis, some steps are taken to the simplified equivalent *LC*-circuit model of the proposed BPF. As depicted in Fig. 3, the input and output probes, whose

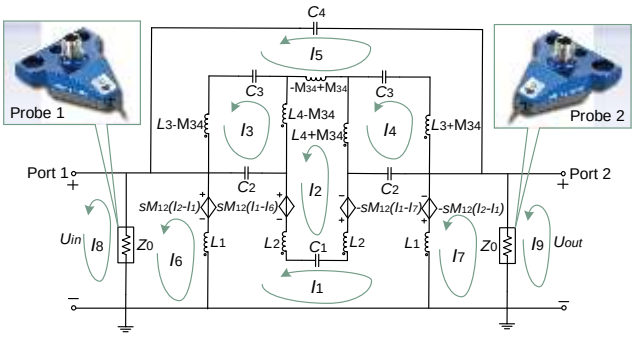

Fig. 3. Schematic of the equivalent circuit model.

impedance values are both 50 Ω, are demonstrated in the circuit and represented as Z_0. Moreover, in order to remove the mutual inductances, an equivalent current-controlled voltage source (CCVS) is introduced to replace the mutual inductance M_{12}. The mutual coupling between the inductors L_3 and L_4 can be decoupled by introducing an additional inductance $|M_{34}|$ in the branch connected to joint point between L_3 and L_4, as shown in Fig. 3. The sign of $|M_{34}|$ is subject to the sign of the coupling coefficient. Then, nine loop currents I_i (i=1, 2, …, 8, 9) are marked in Fig. 3. The coupling coefficients of the Part 1 and Part 2 of the equivalent *LC*-circuit model are opposite, since the assumed directions of the loop currents flowing through the lumped inductors L_1 and L_2 are opposite. The relationship between the coupling coefficient K and mutual inductance M can be expressed as follows [21]:

$$K_{ij} = \frac{M_{ij}}{\sqrt{L_i \times L_j}} \tag{1}$$

where L_i and L_j denote self-inductances of two inductors, M_{ij} and K_{ij} are mutual inductance and coupling coefficient between them (i, j=1, 2, 3, 4), respectively. Therefore, the mutual inductance values of the Part 1 and Part 2 of the equivalent *LC*-circuit model are opposite. Then, a simplified equivalent circuit model can be obtained by removing the magnetic coupling between the coupled inductors, as shown in Fig. 3.

The frequencies of TZs and TPs can be calculated based on the transfer function of the equivalent circuit model of Fig. 3. Applying Kirchhoff's voltage law (KVL), the voltage equations of the nine loops are expressed as:

$$(I_6 - I_8)Z_0 - U_{in} = 0 \tag{2}$$

$$sM_{12}(I_2 - I_1) + sL_1(I_1 - I_6) - Z_0(I_6 - I_8) = 0 \tag{3}$$

$$2s(L_1+L_2)I_1 + \frac{2I_1}{sC_2} + \frac{I_1}{sC_1} + sM_{12}(I_1 - I_7) - sL_1I_6 - sM_{12}(I_1 - I_6) - 2sL_2I_2 - \frac{I_2}{sC_1} - \frac{I_3}{sC_2} - \frac{I_4}{sC_2} = 0 \tag{4}$$

$$sM_{12}(I_2 - I_1) + sL_1(I_7 - I_1) + Z_0(I_7 - I_9) = 0 \tag{5}$$

$$\frac{I_3}{sC_2} + \frac{I_3}{sC_3} + s(L_3+L_4-2M_{34})I_3 - \frac{I_5}{sC_3} - s(L_3-M_{34})I_5 - s(L_4-M_{34})I_2 - \frac{I_1}{sC_2} = 0 \tag{6}$$

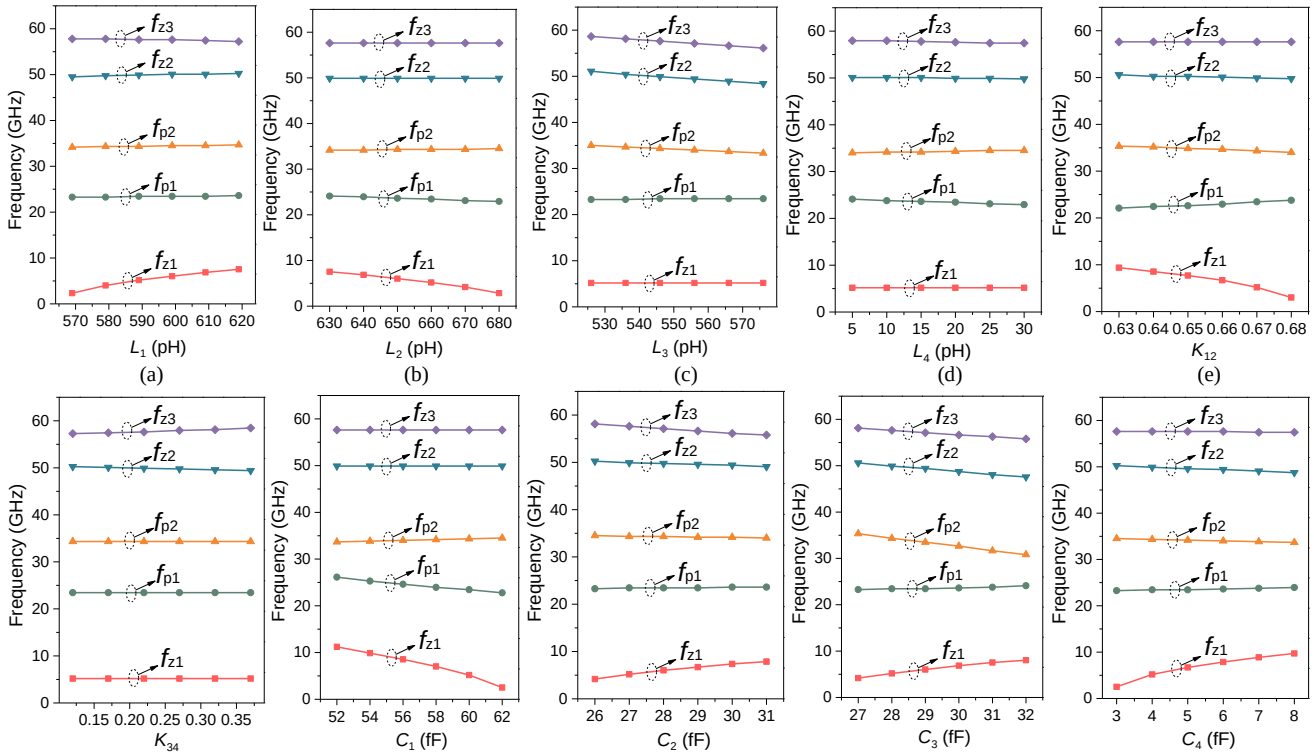

Fig. 4. Resonant frequencies of the transmission zeros and poles of the presented BPF by varying (a) L_1, (b) L_2, (c) L_3, (d) L_4, (e) K_{12}, (f) K_{34}, (g) C_1, (h) C_2, (i) C_3 and (j) C_4.

$$\frac{I_4}{sC_2}+\frac{I_4}{sC_3}+s(L_3+L_4+2M_{34})I_4-\frac{I_5}{sC_3} \\ -s(L_3+M_{34})I_5-s(L_4+M_{34})I_2-\frac{I_1}{sC_2}=0 \tag{7}$$

$$sM_{12}(I_1-I_6)-sM_{12}(I_1-I_7)+2sL_2I_2+\frac{I_2}{sC_1}+2sL_4I_2 \\ -2sL_2I_1-\frac{I_1}{sC_1}-s(L_4-M_{34})I_3-s(L_4+M_{34})I_4=0 \tag{8}$$

$$2sL_3I_5+\frac{2I_5}{sC_3}+\frac{I_5}{sC_4}-\frac{I_3}{sC_3}-\frac{I_4}{sC_3}-s(L_3-M_{34})I_3-s(L_3+M_{34})I_4=0 \tag{9}$$

$$U_{out}+(I_7-I_9)Z_0=0 \tag{10}$$

where U_{in} and U_{out} denote the input and output voltages, respectively. s is a complex variable in proportion to angular frequency ω. Therefore, the transfer function of the equivalent circuit model in Fig. 3 can be written as: [21]

$$G(s)=\frac{U_{out}(s)}{U_{in}(s)}=\frac{U_{out}(j\omega)}{U_{in}(j\omega)} \tag{11}$$

where ω denotes angular frequency and j is a pure imaginary unit number. Using MATLAB, the transfer function represented by complex variable s, coupling coefficients K_{ij} and lumped LC-elements can be deduced by solving equations (2)-(10). Then, the numerator and denominator of the transfer function are extracted. The frequencies of TZs and TPs can be calculated by solving the equations $U_{out}(j\omega) = 0$ and $U_{in}(j\omega) = 0$, respectively. Therefore, three TZs f_{zi} (i=1,2,3) and two TPs f_{pi} (i=1,2) can be obtained through the calculations.

D. Distribution of Transmission Zeros and Poles

To understand the impact of the coupling coefficients and lumped components on the distribution of the TZs and TPs, the frequency responses of TZs and TPs versus different values of the lumped elements and coupling coefficients are exhibited in Fig. 4. For summary, Table Ⅱ is provided, where the gray blocks mean that TZ or TP remains almost unchanged with a varying parameter of coupling coefficient K_{ij} or lumped LC-element. The yellow blocks mean that when the parameter rises up, the TZ or TP has a slight variation. Furthermore, red or green blocks represent the positive or negative correlation between the parameters and TZ or TP, respectively. Table II gives an overall demonstration about the distributions of the TZs and TPs, which are useful to understand the center frequency specification, bandwidth control and stopband attenuation.

TABLE Ⅱ
RELATIONSHIPS BETWEEN PARAMETERS AND TZS OR TPS

	L_1	L_2	L_3	L_4	K_{12}	K_{34}	C_1	C_2	C_3	C_4
f_{z1}	↗	↘	—	—	↘	—	↘	↗	↗	↗
f_{p1}	—	↘	—	↘	↗	—	↘	↗	↗	↗
f_{p2}	↗	—	↘	—	↘	—	↗	—	↘	↘
f_{z2}	↗	—	↘	—	↘	↘	—	↘	↘	↘
f_{z3}	↘	—	↘	↘	↘	↗	—	↘	↘	—

—: not much impact; ↗: positive correlation; ↘: negative correlation.

To obtain the mathematical expressions of the TZs and TPs, the assumption has to be made by eliminating the components having less impact on the resonant frequencies in $U_{out}(j\omega)$ and $U_{in}(j\omega)$. According to Table II, the components highlighted in gray and yellow are removed for f_{zi} (i=1,2,3) and f_{pi} (i=1,2), respectively.

Since $s=j\omega=j2\pi f$, the three TZs f_{zi} (i=1,2,3) and two TPs f_{pi} (i=1,2) can be obtained by solving the equations $U_{out}(j\omega) = 0$ and $U_{in}(j\omega) = 0$, respectively. Finally, the expressions of three TZs and two TPs are obtained as (12)-(16):

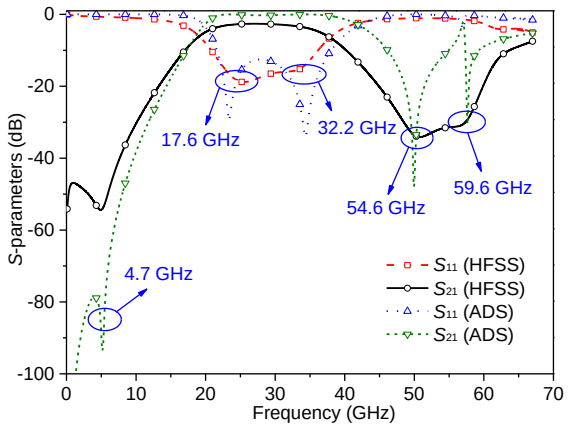

Fig. 5. Simulated frequency responses of the BPF (by HFSS) and the simplified equivalent *LC*-circuit in Fig. 2(b) (by ADS, where L_1= 589 pH, L_2=660 pH, L_3=546 pH, L_4=20 pH, M_{12}=421pH, M_{34}= 23pH, C_1=60 fF, C_2=27 fF, C_3=28 fF, C_4=4 fF).

$$f_{z2}=\frac{\sqrt{C_3L_3(C_2+2C_4)(C_2+C_3+2C_4)}}{2\pi(C_2C_3L_3+2C_3C_4L_3)} \tag{12}$$

$$f_{z3}=\frac{\sqrt{C_2C_3L_4(M_{34}^2-L_3L_4)(C_2+C_3)}}{2\pi j(C_2C_3M_{34}^2-C_2C_3L_3L_4)} \tag{13}$$

Substituting the values of the lumped elements and coupling coefficients in (12)-(16) with the ones extracted from the simulation results in ADS, the estimated TZs and TPs are 4.9 GHz, 54.6 GHz, 59.6 GHz, 17.6 GHz and 32.2 GHz, respectively. To validate the calculated results above, the simulation results of the EM structure and the proposed equivalent *LC*-circuit model are compared with the calculated ones, as shown in Fig. 5, where the EM simulation result was achieved by HFSS and the schematic simulation one was achieved by ADS. It is obvious that the simulated results of equivalent *LC*-circuit model of the BPF can match the ones of the EM structure. The difference between the schematic and EM simulated results are likely due to the discrepancies of the quality factors between the ideal components and EM structure, where the lumped components are lossless elements in the schematics. In terms of the calculated ones, although there are some frequency mismatches, due to the assumption condition

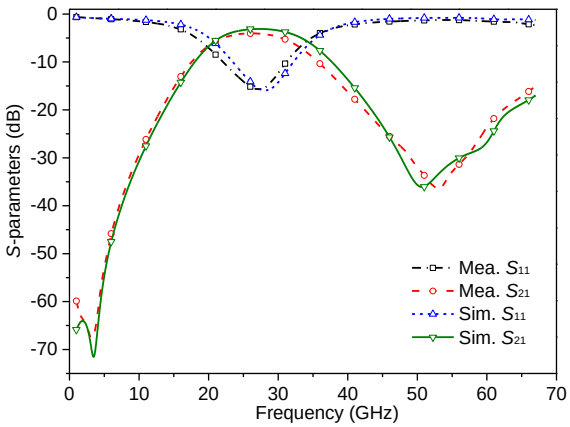

Fig. 6. Simulated and measured frequency responses of the BPF.

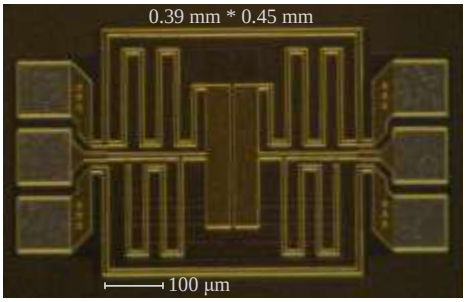

Fig. 7. Die photo of the proposed BPF.

made during calculation by removing the less related elements, the calculated results still agree well with the simulated ones.

III. Measurement Results

The performance of the designed BPF is measured via an on-wafer G-S-G probing from 1 GHz up to 67 GHz with the help of a vector network analyzer E8361A and N5260-60003 from Agilent. As demonstrated in Fig. 6, compared with the simulated results achieved by HFSS, the measured insertion loss and return loss are 3.8 dB and 15.8 dB at the center of 26.5 GHz, respectively. A 3-dB bandwidth is achieved from 19.7 GHz to 33.2 GHz. The Thru–reflect–line (TRL) calibration structures were fabricated on the same chip and used for de-embedding. Besides, a die photo of the designed BPF is shown in Fig. 7. Excluding the testing pads, the size of the chip

$$f_{z1}=\frac{\sqrt{\sqrt{2}C_1L_1(M_{12}^2-L_1L_2)(C_2+C_3+2C_4)(C_2L_1^2+C_3L_1^2+2C_4L_1^2-2C_1M_{12}^2)}}{2\sqrt{2}\pi j(C_1C_2L_1^2L_2+C_1C_3L_1^2L_2+2C_1C_4L_1^2L_2-C_1C_2L_1M_{12}^2-C_1C_3L_1M_{12}^2-2C_1C_4L_1M_{12}^2)} \tag{14}$$

$$f_{p1}=\sqrt{\frac{2C_1L_2-\sqrt{4C_1^2L_2^2+8C_1^2L_2L_4+4C_1^2L_4^2-4C_1C_2L_2L_4+4C_1C_2L_4^2+C_2^2L_4^2}+2C_1L_4+C_2L_4}{16\pi^2C_1C_2L_2L_4}} \tag{15}$$

$$f_{p2}=\sqrt{\frac{C_3L_1-\sqrt{(C_3^2L_1^2+4C_3^2L_1L_3+4C_3^2L_3^2+4C_3C_4L_1^2-8C_3C_4L_1L_3+4C_4^2L_1^2}+2C_4L_1+2C_3L_3}{-16\pi^2C_3C_4L_1L_3}} \tag{16}$$

TABLE Ⅲ
PERFORMANCE COMPARISONS BETWEEN THIS WORK AND SOME OTHER WORKS

Ref.	f_c (GHz)	3-dB BW (%)	Insertion Loss (dB)	TZ	TP	Area (λ_g^2)	Harmonic Rejection (dB)	Technology	Order of BPF	Technique
[5]	64	18.8	4.9	2	2	0.096	57	0.18-μm CMOS	1	Capacitive coupling
[9]	58.3	26.6	4	2	2	0.029	26	0.18-μm CMOS	1	Magnetic coupling
[12]	35	N.A.	4.5	2	2	0.007	49	0.18-μm CMOS	1	Capacitive coupling
[13]	60	17	4.1	4	2	0.047	49	0.13-μm SiGe	2	N.A.
[18]	59.5	21.7	3.3	2	2	0.009	18	0.18-μm CMOS	1	Magnetic coupling
[20]	23.5	22.2	2.9	1	2	0.013	40	0.1-μm GaAs	2	Magnetic coupling
This work	**26.5**	**50.9**	**3.8**	**3**	**2**	**0.005**	**36**	**0.13-μm SiGe**	**1**	**Hybrid Coupling**

is 0.39 × 0.45 mm^2. The performance comparisons between this work and some other state-of-the-art designs are illustrated in Table Ⅲ. As can be seen, the designed BPF has the merits of multiple transmission zeros and poles with a compact size.

IV. CONCLUSION

In this paper, using hybrid coupling technique, a compact on-chip BPF is designed and analyzed. Three TZs and two TPs are generated by the presented single-element structure. In addition, the bandwidth and center frequency of the designed BPF can be tuned in a flexible way by simply adjusting the corresponding lumped elements or coupling coefficient in the equivalent *LC*-circuit model. Solving the transfer function of the circuit model, the expressions of TPs and TZs can be estimated for flexible control of the passband and stopband the bandwidth. An EM simulator is used to optimize the dimension of BPF. The designed BPF is implemented and fabricated in a standard 0.13-μm SiGe (Bi)-CMOS technology. Good agreement between the simulated and measured results has been obtained. Based on the results, we could conclude that the presented approach can be used as a guideline for passive device implementation, where coupling between metal strips play a dominant role, such as BPF.

REFERENCES

[1] C. W. You and Y. S. Lin, "Miniature on-chip bandpass power divider with equalripple response and wide upper stopband," *IET Microw., Antennas Propag.*, vol. 6, no. 13, pp. 1461–1467, 2012. (DOI: 10.1049/iet-map.2012.0091)

[2] H. Chuang, L. Yeh, P. Kuo, K. Tsai and H. Yue, "A 60-GHz millimeter-wave CMOS integrated on-chip antenna and bandpass filter," *IEEE Trans. Electron Devices*, vol. 58, no. 7, pp. 1837–1845, Jul. 2011. (DOI: 10.1109/TED.2011.2138141)

[3] H. Chiou and I. Chen, "High-efficiency dual-band on-chip rectenna for 35- and 94-GHz Wireless Power Transmission in 0.13-m CMOS technology," *IEEE Trans. Microw. Theory Tech.*, vol. 58, no. 12, pp. 3598–3606, Dec. 2010. (DOI: 10.1109/TMTT.2010.2086350)

[4] Z. Zhang and X. Liao, "Micromachined passive bandpass filters based on GaAs monolithic-microwave-integrated-circuit technology," *IEEE Trans. Electron Devices*, vol. 60, no. 1, pp. 221–228, Dec. 2012. (DOI: 10.1109/TED.2012.2228197)

[5] C. Hsu, C. Chen, and H. Chuang, "A 60-GHz millimeter-wave bandpass filter using 0.18-μm CMOS technology," IEEE Electron Device Lett., vol. 29, no. 3, pp. 246–248, Feb. 2008. (DOI: 10.1109/LED.2007.915369)

[6] N. Zhang, L. Mei, C. Wang, Z. Deng, J. Yang, and Q. Guo, "A switchable bandpass filter employing RF MEMS switches and open-ring resonators," *IEEE Trans. Electron Devices*, vol. 64, no. 8, pp. 3377–3383, Aug. 2017. (DOI: 10.1109/TED.2017.2712643)

[7] L. Li, W. Shen, J. Ding, and X. Sun, "Compact 60-GHz on-chip bandpass filter with low insertion loss," *IEEE Electron Device Lett.*, vol. 39, no. 1, pp. 12–14, Dec. 2017. (DOI: 10.1109/LED.2017.2778714)

[8] N. Mahmoud, A. Barakat, A.B. Abdel-Rahman, A. Allam and R.K. Pokharel, "Compact size on-chip 60 GHz H-shaped resonator BPF," *IEEE Microw. Wireless Compon. Lett.*, vol. 26, no. 9, pp. 681–683, Sep. 2016. (DOI: 10.1109/LMWC.2016.2597219)

[9] K. Ma, S. Mou, and K. Seng Yeo, "Miniaturized 60-GHz on-chip multimode quasi-elliptical bandpass filter," *IEEE Electron Device Lett.*, vol. 34, no. 8, pp. 945–947, Aug. 2013. (DOI: 10.1109/LED.2013.2265165)

[10] J. Hoffman, J. Martin-Gosse, S. Shopov, J. J. Pekarik, R. Camillo-Castillo, V. Jain, D. Harame, and S. P. Voinigescu, "Analog Circuit Blocks for 80-GHz Bandwidth Frequency-Interleaved, Linear, Large-Swing Front-Ends," *IEEE Journal of Solid-State Circuits*, vol. 51, no. 9, pp. 1985-1993, Sep. 2016. (DOI: 10.1109/JSSC.2016.2567445)

[11] S. Sun, J. Shi, L. Zhu, S. C. Rustagi, and K. Mouthaan, "Millimeter-Wave Bandpass Filters by Standard 0.18-μm CMOS Technology," *IEEE Electronic Device Letters*, vol. 28, no. 3, pp. 220-222, Mar. 2007. (DOI: 10.1109/LED.2007.891305)

[12] L. Yeh, C. Chen, and H. Chuang, "A millimeter-wave CPW CMOS on-chip bandpass filter using conductor-backed resonators," *IEEE Electron Device Lett.*, vol. 31, no. 5, pp. 12–14, May. 2010. (DOI: 10.1109/LED.2010.2043333)

[13] A. Franc, E. Pistono, D. Gloria, and P. Ferrari, "High-performance shielded coplanar waveguides for the design of CMOS 60-GHz bandpass filters," *IEEE Trans. Electron Devices*, vol. 59, no. 5, pp. 1219–1226, May. 2012. (DOI: 10.1109/TED.2012.2186301)

[14] Z. Gao, K. Kang, Z. Jiang, Y. Wu, C. Zhao, Y. Ban, L. Sun, Q. Xue and W. Yin, "Analysis and equivalent-circuit model for CMOS on-chip multiple coupled inductors in the millimeter-wave region," *IEEE Trans. Electron Devices*, vol. 62, no. 12, pp. 3957–3964, Dec. 2015. (DOI: 10.1109/TED.2015.2488840)

[15] Y. Yang, H. Liu, Z. Hou, X. Zhu, E. Dutkiewicz, and Q. Xue, "Compact on-chip bandpass filter with improved in-band flatness and stopband attenuation in 0.13-μm (Bi)-CMOS technology," *IEEE Electron Device Lett.*, vol. 38, no. 10, pp. 1359–1362, Oct. 2017. (DOI: 10.1109/LED.2017.2739186)

[16] Y. Zhong, Y. Yang, X. Zhu, E. Dutkiewicz, K. Shum and Q. Xue, "An on-chip bandpass filter using a broadside-coupled meander line resonator with a defected-ground structure," *IEEE Electron Device Lett.*, vol. 38, no. 5, pp. 626–629, May. 2017. (DOI: 10.1109/LED.2017.2690283)

[17] S. Chakraborty, Y. Yang, X. Zhu, O. Sevimli, Q. Xue, K. Esselle and M. Heimlich, "A broadside-coupled meander-line resonator in 0.13-μm SiGe technology for millimeter-wave application," *IEEE Electron Device Lett.*, vol. 37, no. 3, pp. 329–332, Mar. 2016. (DOI: 10.1109/LED.2016.2520960)

[18] A. El-Hameed, A. Barakat, A. Abdel-Rahman, A. Allam, and R. Pokharel "Ultracompact 60-GHz CMOS BPF employing broadside-coupled open-loop resonators," *IEEE Microw. Wireless Compon. Lett.*, vol. 27, no. 9, pp. 818–820, Sep. 2017. (DOI: 10.1109/LMWC.2017.2734771)

[19] Y. Yang, X. Zhu, and Q. Xue, "Design of an ultracompact on-chip bandpass filter using mutual coupling technique," *IEEE Trans. Electron Devices*, vol. 65, no. 3, pp. 1087–1093, Mar. 2018. (DOI: 10.1109/TED.2018.2797304)

[20] Y. Yang, X. Zhu, E. Dutkiewicz, and Q. Xue, "Design of a miniaturized on-chip bandpass filter using edge-coupled resonators for millimeterwave

applications," *IEEE Trans. Electron Devices*, vol. 64, no. 9, pp. 3822–3828, Sep. 2017. (DOI: 10.1109/TED.2017.2720185)

[21] C. Alexander and M. Sadiku, *Fundamentals of Electric Circuits.* New York, NY, USA: McGraw-Hill Education, 5th Edition 2012.